Journal of Power Sources 221 (2013) 318–327

Contents lists available at SciVerse ScienceDirect

Journal of Power Sources

journal homepage: www.elsevier.com/locate/jpowsour

Short communication

Fabrication of novel phosphotungstic acid functionalized mesoporous silica composite membrane by alternative gel-casting technique

Lan Zhang [a,b,*], Hong Quan He [b], Raj Kamal S/O Abdul Rasheed [b,c], Wei Jiang Zhou [b], Yan Hong Xue [b], Ovi Lian Ding [b], Siew Hwa Chan [a,b,c,**]

[a] Temasek Laboratories @NTU, Nanyang Technological University, 50 Nanyang Drive, Singapore 637553, Singapore
[b] Energy Research Institute @NTU, Nanyang Technological University, 50 Nanyang Drive, Singapore 637553, Singapore
[c] School of Mechanical and Aerospace Engineering, Nanyang Technological University, 50 Nanyang Avenue, Singapore 639798, Singapore

HIGHLIGHTS

- HPW/MCM-41 composite membranes have been fabricated by a gel-casting technique.
- HPW/MCM-41 composite membranes can operate stably below 200 °C.
- A single cell can be assembled using the HPW/MCM-41 membrane.
- A maximum output power density of 101 mW cm^{-2} in MeOH/air at 150 °C was observed.

ARTICLE INFO

Article history:
Received 16 May 2012
Received in revised form
15 July 2012
Accepted 31 July 2012
Available online 24 August 2012

Keywords:
Direct methanol fuel cell
Phosphotungstic acid
Mesoporous silica
Gel-casting
High-temperature proton exchange membranes

ABSTRACT

A simple and cost-effective gel-casting technique has been developed to fabricate phosphotungstic acid (HPW) supported on mesoporous silica (MCM-41) electrolyte membrane (HPW/MCM-41) for direct methanol fuel cells (DMFCs). The effect of HPW loading on the stability of MCM-41 structure has been analyzed by small-angle X-ray scattering (SAXS), Fourier transform infrared (FTIR), thermogravimetric analysis (TGA) and derivative thermogravimetry (DTG) techniques. In particular, the effect of solid state loading and HPW loading on the microstructure, water gain ratio, swelling ratio and conductivity of the HPW/MCM-41 membranes have been studied in detail. The results showed that a large proportion of loaded HPW is anchored in the mesoporous silica matrix, forming an effective proton conduction pathway. The results also showed that the composite membrane can operate successfully at temperatures below 200 °C for a long duration, based on the TGA curve of organic network formed during the gelation stage. The single cell assembled from HPW/MCM-41 membrane with 65 wt.% HPW loading gives a peak power of 101 mW cm^{-2} in methanol/air at 150 °C without any humidification.

1. Introduction

The proton exchange membrane fuel cell (PEMFC) has been proved to be an alternative power source compared to the internal combustion engines, especially for portable power and automobile applications. However, PEMFC relies exclusively on pure hydrogen, which is not readily available for widespread application. Though fuel reforming technology is rather mature, matching of fuel reformer to the fuel cell stack adds on to the cost significantly, especially for subsequent gases cleanup and purification, which would make the PEMFC system very bulky and maintenance hassle. Much different from the direct methanol fuel cell (DMFC) that operates at around the room temperature, high-temperature PEMFC (HT-PEMFC) has evolved very rapidly in recent years. It is seen to be a promising technology that is able to penetrate the market for practical application as methanol/ethanol can be used directly or even logistic fuels that can be applied with a simple fuel reforming technique. The main advantages of operating HT-PEMFC at temperatures above 150 °C include fuel flexibility, improved resistance to carbon monoxide poisoning and the ability of using of non-Pt catalyst. These advantages also prompt some new challenges such as the reliability of conductivity of PEM, low-cost non-

* Corresponding author. Temasek Laboratories @NTU, Nanyang Technological University, 50 Nanyang Drive, Singapore 637553, Singapore. Tel.: +65 6790 5591; fax: +65 6790 5591.
** Corresponding author. Energy Research Institute @NTU, Nanyang Technological University, 50 Nanyang Drive, Singapore 637553, Singapore.
E-mail addresses: zhanglan@ntu.edu.sg (L. Zhang), mshchan@ntu.edu.sg (S.H. Chan).

0378-7753/$ – see front matter © 2012 Elsevier B.V. All rights reserved.
http://dx.doi.org/10.1016/j.jpowsour.2012.07.131

Pt or low-Pt loading catalyst technology and robust catalyst support resistance to oxidation at elevated temperatures. The proton conductivity of the state-of-the-art perfluorosulfonic acid (PFSA) membranes, such as Nafion, depends strongly on the water content in the membrane. The conductivity decreases with increasing temperature due to the dehumidification effect of the membrane under high temperatures [1–4]. Therefore, the development of proton exchange membranes with high conductivity and stability at high temperature and low humidity form the objective of this study. Many inorganic-based proton conductors have been explored as the electrolytes for HT-PEMFCs, such as heteropoly acid (HPA)-based composite [5–12], ammonium polyphosphate (APP)-based composite [13–24], and doped SnP_2O_7 [25–30]. Among these solid inorganic proton conductive electrolyte materials, HPA, which takes the form of Keggin structure with general formula $H_3MX_{12}O_{40}$ where M = P, Si, etc., and X = W, Mo, V, etc. [7, 31–36]. The highest stability and strongest acidity is observed for phosphotungstic acid ($H_3PW_{12}O_{40}$, HPW). HPW exhibits interesting acid properties due to its easily accessible and reactive protons present in the structure. Although earlier effort on this material as a potential solid electrolyte has failed to meet the requirements due to its high solubility in water and strong humidity-dependent proton conductivity [37], it is interesting to note that the proton conductivity of a well dispersed HPW impregnated into mesoporous silica system by vacuum assisted impregnation method has been quite promising at low humidity [5]. Apart from the conductivity, another technical challenge for the inorganic proton conductive electrolyte is the formation of thin and dense membrane structure with high mechanical strength.

There are various processing techniques available for the fabrication of inorganic proton conductive composite membranes (see Table 1). Till now, there is no report on the inorganic proton conductive composite membrane made by novel ceramic molding technique, i.e., the water-based gel-casting. Gel-casting was first reported by Omatete et al. [38] in 1991. In this technique, slurry of high solid state loading is obtained by dispersing the ceramic powders in the premixed mono-functional and di-functional monomers solution and casted into any desired shape by a mold. By heating or adding catalyst, cross-linking and solidification occur and form a three-dimensional polymeric network structure. Polymerization solidifies and immobilizes the powder into the desired shape. Gel-casting is a low-cost technique commonly used in ceramic industry to fabricate complex three-dimensional ceramic parts [38–40]. Recently, the gel-casting technique has been used to prepare components of solid oxide fuel cells (SOFCs) such as NiO/YSZ (yttria-stabilized zirconia) anode substrates [41]. Due to its simplicity and low-cost, the technique has also been employed in the production of electrode and electrolyte powders for SOFCs [42–47]. It is very inspiring that the phase formation temperature of electrode and electrolyte powders for SOFCs was reported to be considerably lower than that synthesized by conventional solid state reaction route, which is attributed to the uniformly distributed raw particles in a polymeric matrix immobilized during the gelation step. Thus, it is worthwhile to investigate the properties of the HPW/mesoporous silica composite membrane fabricated by the novel ceramic molding technique.

In this paper, a novel HPW-impregnated MCM-41 composite membrane fabricated by an aqueous based gel-casting technique is presented. The effects of HPW loading on the structural stability of MCM-41, the thermal stability of as-assembled powders, the proton conductivity, stability and microstructure of HPW/MCM-41 composite membranes, and the cell performance are investigated in detail.

2. Experimental procedure

2.1. Assembled powders preparation

A large quantity of mesoporous silica MCM-41 was synthesized based on a previously reported procedure [48,49]. Phosphotungstic acid (HPW) was ordered from Sigma–Aldrich. The as-assembled HPW/MCM-41 powders were prepared by a vacuum assisted impregnation method [5]. MCM-41 was treated under vacuum ($<10^{-1}$ Pa) to remove impurities and trapped air in the mesoporous

Table 1
Inorganic proton conductors, fabrication method of composite membranes.

Entry	Proton conductors	Additional organic	Additional inorganic	Fabrication method	Ref.
1	HPW	–	Meso-silica	Pressing	[5]
2	HPW	–	Meso-silica	Pressing	[6]
5	HPW	Polyimide	Meso-silica	Pressing	[12]
6	HPW	Nafion	ZrO_2	Casting	[7]
7	HPW	Polybenzimidazole	Silica	Casting	[8]
8	HPW	Nafion	Silica	Recasting	[9]
9	HPW	Sulfonated poly(ether sulfone)	Silica	Casting	[10]
10	HPW	Perfluorosulfonic acid	Silica	Casting	[11]
11	$(NH_4)_2Si_{1-x}Ti_xP_4O_{13}(0 \leq x \leq 1)$	–	–	Pressing	[14]
12	$(NH_4)_2SnP_4O_{13}$	–	–	Pressing	[15]
13	$2NH_4PO_3$-$(NH_4)_2SiP_4O_{13}$ $2NH_4PO_3$-$(NH_4)_2Mn(PO_3)_4$	–	–	Pressing	[16]
14	NH_4PO_3-$(NH_4)_2Mn(PO_3)_4$	–	–	Pressing	[17]
15	NH_4PO_3	–	Silica	Pressing	[18]
16	NH_4PO_3-$(NH_4)_2SiP_4O_{13}$	–	–	Pressing	[19]
17	$(NH_4)_2SiP_4O_{13}$	–	–	Pressing	[20]
18	NH_4PO_3-$(NH_4)_2SiP_4O_{13}$	–	–	Pressing	[21]
19	NH_4PO_3	Poly(tetrafluoroethylene) (PTFE)	–	Pressing	[22]
20	NH_4PO_3	–	Amorphous oxide $SiO_2 - P_2O_5$	Pressing	[23]
21	$(NH_4)_2TiP_4O_{13}$	–	–	Pressing	[24]
22	$Sn_{0.9}In_{0.1}P_2O_7$	–	–	Pressing	[25]
23	$Sn_{0.9}In_{0.1}P_2O_7$	Poly(tetrafluoroethylene) (PTFE)	–	Cold-rolling	[26]
24	$Sn_{0.9}In_{0.1}P_2O_7$	Poly(tetrafluoroethylene) (PTFE) Polybenzimidazole (PBI)	–	Cold-rolling	[27]
25	$Sn_{0.9}In_{0.1}P_2O_7$	–	–	Pressing	[30]

structure, and subsequently it was added to an HPW solution under vacuum. The powders were dried at 90 °C for 20 h and collected. The samples containing 15, 30, 50, 65 and 80 wt.% of HPW in as-assembled powders are marked as MCM-41-HPW15, MCM-41-HPW30, MCM-41-HPW50, MCM-41-HPW65 and MCM-41-HPW80, respectively.

2.2. Membrane preparation

As-assembled HPW/MCM-41 powders were mixed into a premixed solution, followed by a planetary ball milling for 10 min. The premixed solution was made by mixing mono-functional acrylic acid, C_2H_3COOH (AC), di-functional N,N′-Methylenebis-acrylamide $(C_2H_3CONH)_2CH_2$ (MBAM), and a dispersant. The mixed slurry was deaired before ammonium persulfate $(NH_4)_2S_2O_8$ (APS, 2 wt.% water solution) was added as an initiator. AC, MBAM and APS were purchased from Sigma–Aldrich. The slurry was poured into glass molds, and subsequently heated in an oven at 90 °C for 45 min. The flow chart and schematic of gel-casting process for HPW/MCM-41 HT-PEM are shown in Figs. 1 and 2, respectively. The optical and microstructure pictures of the resulting gel sheet, i.e., the membrane, are shown in Fig. 3. As shown in Fig. 3, the thickness of the membrane is ∼450 μm. The membranes fabricated from MCM-41, MCM-41-HPW15, MCM-41-HPW30, MCM-41-HPW50, MCM-41-HPW65 and MCM-41-HPW80 powders shall be denoted as MCM-41-m, MCM-41-HPW15-m, MCM-41-HPW30-m, MCM-41-HPW50-m, MCM-41-HPW65-m and MCM-41-HPW80-m, respectively. Poly(acrylic acid) (PAA) was prepared by polymerization of acrylic acid and cross-link agent at 90 °C for 45 min. The chemical reagents mentioned are directly used as-is without further purification treatment.

2.3. As-assembled powders and membranes characterization

Small-angle X-ray scattering (SAXS) patterns of as-assembled HPW/MCM-41 powders were recorded on a PANalytical diffractometer (model: Empyrean 9430.060.03002) with a CuKα (λ = 1.5406 Å) radiation operating at 40 kV, 40 mA under room environment.

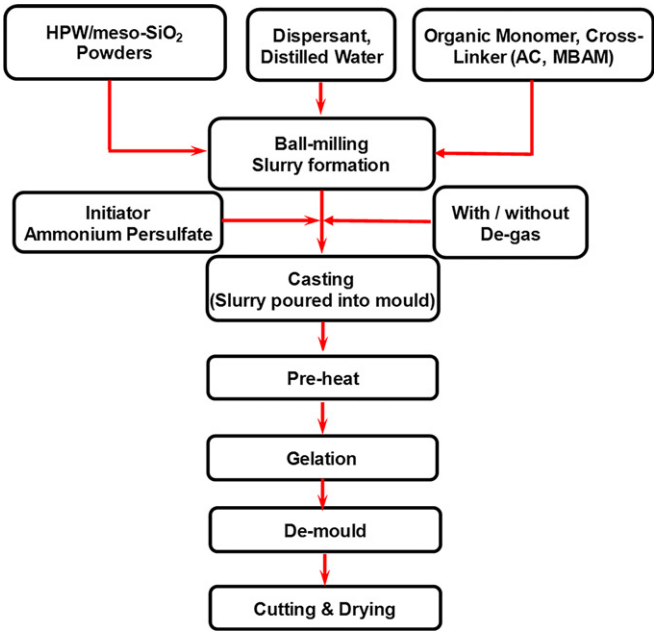

Fig. 1. Flow chart of gel-casting process for MCM-41-HPW-m membranes.

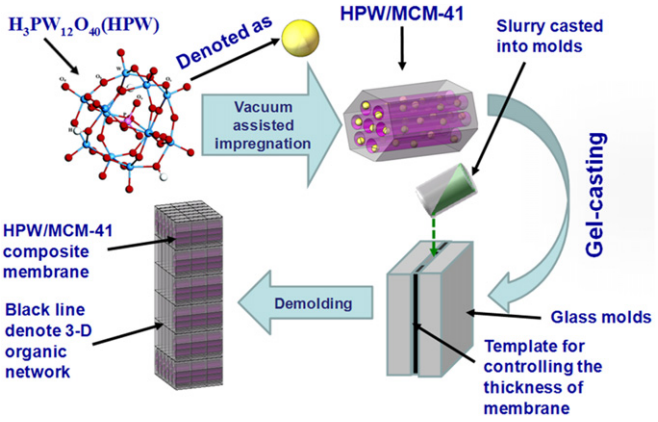

Fig. 2. Schematic drawing of vacuum assisted impregnation method for MCM-41-HPW composite powders and gel-casting process for MCM-41-HPW-m membrane fabrication.

Fourier transform infrared (FTIR) absorption spectra of the pure HPW and as-assembled HPW/MCM-41 powders were obtained using the Perkin Elmer Spectrum GX (spectral range of 4000–200 cm^{-1}, 50 scans, resolution of 2 cm^{-1}). The samples were diluted in KBr (10 wt.% sample and 90 wt.% KBr) and were pressed into thin wafers for analysis.

Thermogravimetric analysis (TGA) and derivative thermogravimetry (DTG) of the MCM-41, HPW, as-assembled HPW/MCM-41 powders and PAA were carried out on a 2950 thermal analyzer (TA Instruments Inc., New Castle, DE) with a heating rate of 10 °C min^{-1} under air flow rate of 60 mL min^{-1}.

The microstructure of HPW/MCM-41 membranes and X-ray energy dispersion spectroscopy (EDS) were examined by a field emission scanning electron microscopy (FESEM, JSM-7600F, JEOL).

The pure water/methanol uptake of the membranes fabricated from slurry with different solid state loading and as-assembled HPW/MCM-41 powders is defined as the mass ratio of absorbed water and methanol to the dry membrane. A water/methanol uptake test was carried out according to the following procedure: the membrane was first vacuum-dried at 100 °C until a constant weight was obtained. The dried membrane (W_{dry}) was then soaked in deionized water/methanol for 24 h at 80 °C. Subsequently, the membranes were taken out and weighed (W_{wet}) using a microbalance after removing surface water/methanol with filtration paper. The water/methanol uptake was calculated using Eq. (1):

$$W_{H_2O/CH_3OH} = \frac{W_{wet} - W_{dry}}{W_{dry}} \times 100\% \quad (1)$$

Swelling ratio of the composite membrane was calculated using Eq. (2):

$$S_{H_2O/CH_3OH} = \frac{A_{wet} - A_{dry}}{A_{dry}} \times 100\% \quad (2)$$

where A_{wet} and A_{dry} are the areas of the dry and wet membrane, respectively.

2.4. Conductivity and cell performance measurements

Proton conductivity measurements of HPW/MCM-41 composite membranes fabricated by gel-casting technique were measured with impedance spectroscopy using Autolab PGSTAT302N/FRA electrochemistry workstation over the frequency range from 1 Hz

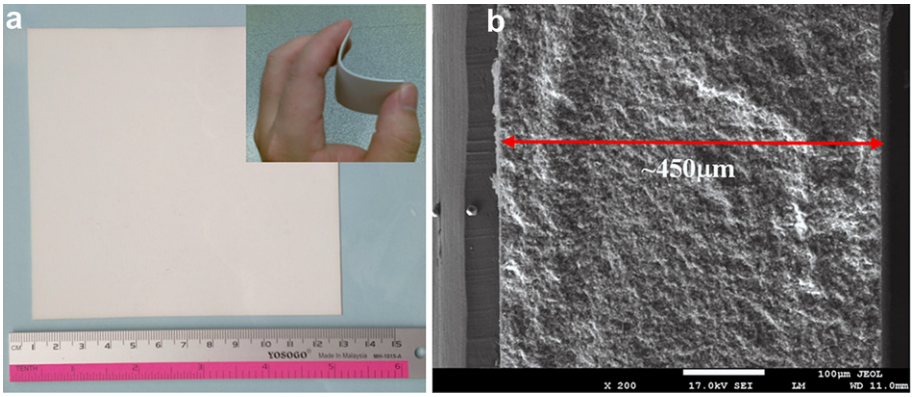

Fig. 3. (a) Optical and (b) cross-sectional microstructure pictures of the MCM-41-HPW-m membrane fabricated by gel-casting process.

to 1 MHz and the temperature range from 20 to 90 °C under 100% relative humidity (RH).

The MCM-41-HPW65-m mesoporous silica composite membrane was sandwiched between anode (direct methanol fuel cell anode, product code: 45374, Johnson Matthey) and cathode (direct methanol fuel cell cathode, product code: 45375, Johnson Matthey) with diffusion layer. The effective electrode area is 4 cm^2. Then the sandwiched structure clamped and sealed between two graphite plates with engraved flow field were used for membrane electrode assembly (MEA) characterization. The flow rate of methanol solution (with concentration of 2.0 mol L^{-1}) was 1 mL min^{-1}, while air flow rate was 300 mL min^{-1} without humidification. The cell performance measurements were carried out in the temperature range from 80 °C to 150 °C. The conductivity stability of the membrane was measured at 80 °C in the same set-up with carbon paper (Toray TGPH-060) under a continuous flow of deionized water at both sides of the membrane.

3. Results and discussion

3.1. SAXS, FTIR spectroscopy and TGA & DTG curves

Fig. 4 shows the results of small-angle X-ray scattering (SAXS) patterns of mesoporous silica with/without HPW impregnation. All samples indicate well-resolved scattering peaks and characteristic SAXS patterns of mesoporous silica. For pristine mesoporous silica, the SAXS curve (black line) shows three-resolved scattering peaks, which can be assigned to the 100, 110 and 200 scattering peaks of the MCM-41 structure, suggesting the successful formation of the large quantity MCM-41 [50,51]. The position of the scattering peaks for HPW/MCM-41 powders remains the same as that of the pristine MCM-41 without any HPW impregnated, indicating that HPW has coalesced well into the mesoporous structure of MCM-41 [5,6]. This is explained by the occurrence of the relative intensities of scattering peaks of the as-assembled HPW/MCM-41 powders, which decreased significantly with the increase of HPW content until the peak disappeared/almost disappeared [6].

The as-assembled MCM-41-HPW powders prepared by vacuum assisted impregnation method were analyzed by FTIR to confirm the presence of Keggin anions on the MCM-41. The $PW_{12}O_{40}^{3-}$ Keggin anion structure consists of a PO_4 tetrahedron surrounded by four W_3O_9 groups formed by edge-sharing octahedral. These groups are connected to each other by corner-sharing oxygen [52,53]. This structure gives rise to different types of oxygen atoms, which are responsible for the signature of IR bands for the Keggin anions between 1100 and 500 cm^{-1} [36]. The FTIR spectra of MCM-41 with/without HPW impregnation are shown in Fig. 5. In the case of pure HPW, there are five characteristic bands observed at 1078, 983, 887, 796 and 593 cm^{-1}, respectively, which are assigned to the stretching vibration of P—O, W═O_t, W—O_c—W, W—O_e—W and the bending vibration of P—O, respectively [36,53]. In the case of pure MCM-41, the FTIR spectrum shows characteristic bands of Si—O—Si at 1092 cm^{-1} for asymmetrical stretching and 801 cm^{-1} for symmetrical stretching. The bands at 966 and 465 cm^{-1} can be assigned to the Si—O symmetrical stretching and twisting, respectively [53,54].

The spectra presented in Fig. 5 show that the small bands at 983 cm^{-1} and 887 cm^{-1} would become more prominent with increasing the HPW loading on MCM-41. This finding is also

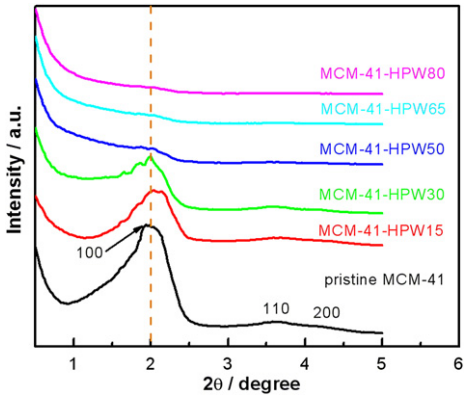

Fig. 4. Small-angle X-ray scattering (SAXS) patterns of MCM-41 and MCM-41-HPW composite powders with different HPW loading.

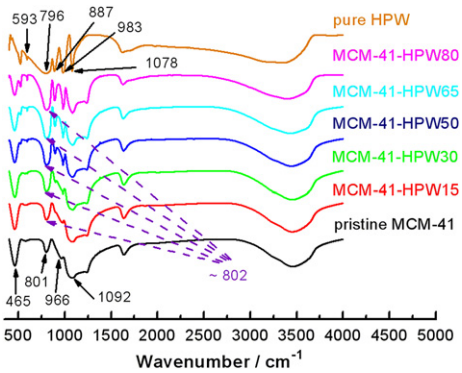

Fig. 5. Fourier transform infrared (FTIR) spectra of HPW, MCM-41, and MCM-41-HPW 637553 composite powders with different HPW loading measured at room temperature.

reported by Khder et al. [53]. Moreover, the intensity of the MCM-41-HPW powders band at around 802 cm^{-1} increases gradually with the HPW loading, which is much more than that of HPW band at 796 cm^{-1} and that of MCM-41 band at 801 cm^{-1}. The increased intensity of the band at ~802 cm^{-1} with the increase in HPW loading can be attributed to the interaction between the Keggin anions of HPW and the silanols on the silica surface to form ($\equiv SiOH_2^+$) ($H_2PW_{12}O_{40}^-$) species [6,55,56].

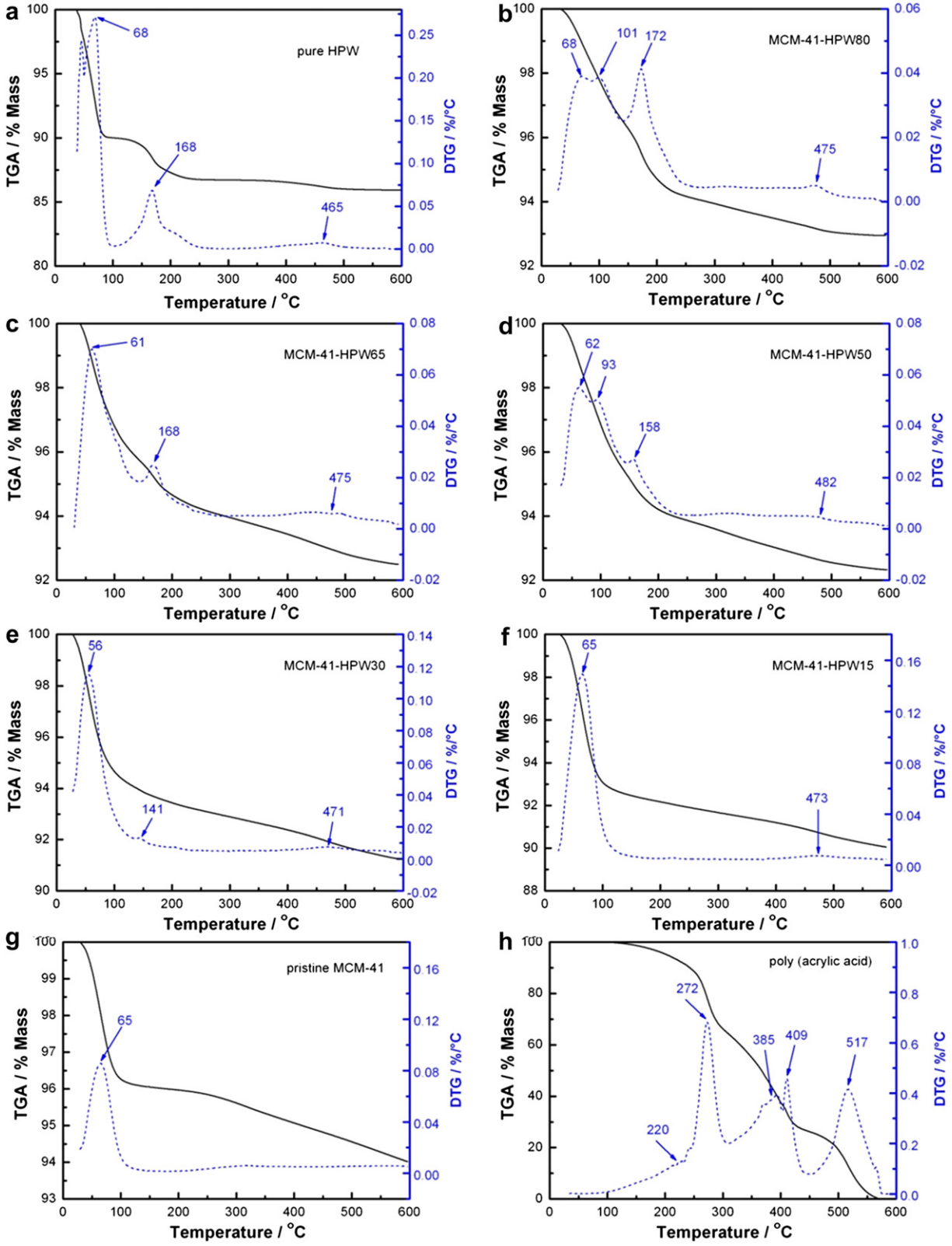

Fig. 6. Thermogravimetric analysis (TGA) and derivative thermogravimetry (DTG) curves of HPW, MCM-41, MCM-41-HPW composite powders with different HPW loading (a) HPW, (b) 80 wt.%, (c) 65 wt.%, (d) 50 wt.%, (e) 30 wt.%, (f) 14 wt.%, (g) pristine MCM-41 and (h) poly (acrylic acid) measured from room temperature up to 600 °C.

Typical thermogravimetric analysis (TGA) and derivative thermogravimetry (DTG) profiles for the pristine MCM-41 powders, pure HPW powders, HPW-impregnated MCM-41 powders, and PAA are shown in Fig. 6. Three distinct weight loss patterns are observed in the pure HPW: the first weight loss of 10% up to 100 °C, the second weight loss of 3.25% up to 250 °C and the third weight loss of 0.83% up to 600 °C (Fig. 6a, the peak of DTG profile in the range of 300–600 °C stood at about 465 °C), which are in agreement with the reported values [57–61]. These weight losses correspond to the loss of non-coordinated water, loss of water of crystallization of Keggin-type anion, and loss of water of condensation (i.e., loss of all acidic protons and the beginning of decomposition of the Keggin structure), respectively [57–61]. The retention of water molecules by the Keggin-type HPW structure at high temperatures indicates the possibility of proton conductivity at elevated temperatures. On the other hand, TGA curve for pristine MCM-41 powders reveals only one weight loss step at ~65 °C, and the weight loss is ~4.0% at 200 °C, which corresponds to the loss of water in the channels of MCM-41 (Fig. 6g) [50,57].

As shown in Fig. 6(b–f), the thermal behavior of HPW-impregnated MCM-41 powders is significantly different from that of pure HPW. A relatively rapid weight loss at first step occurred in the cases of HPW-impregnated MCM-41 powders are due to the loss of water in the channels of MCM-41 and non-coordinated water of HPW. The relative intensity of second weight loss peaks between 100 and 250 °C of HPW decreases with decreasing HPW loading, and nearly disappear when HPW loading is 30 wt.% or less, which is due to all the HPW molecules are moved into the channel of MCM-41 and react with silanols on the silica surface to form ($\equiv SiOH_2^+$) ($H_2PW_{12}O_{40}^-$) when the HPW loading is lower. Thus, the gradual weight loss can be attributed to the difficulty in water removal in ($\equiv SiOH_2^+$) ($H_2PW_{12}O_{40}^-$) [6,56,57]. On the other hand, the second weight loss peaks become stronger with increasing HPW loading up to 80 wt.%, which can be attributed to the pore volume limitation of MCM-41, the excessive HPW absorbed on the surface of MCM-41 or just mixed with MCM-41 [53].

TGA curve for the PAA sample (dried at 150 °C overnight) reveals four main weight loss regions. The first small region (~8 wt.% loss) at temperatures below 230 °C is due to the evaporation of physically weakly and chemically strongly bounded H_2O. The second transition region around 230–300 °C is due to the stripping hydroxyl and carboxylic acid functional groups in the branched chain of PAA polymer. The total weight loss at this stage is about 26 wt.%. The transition peaks of third and fourth stages after 300 °C are attributed to the cleavage backbone of polymer [62,63].

In summary, the results indicate that MCM-41-HPW membranes fabricated by gel-casting technique can operate up to 200 °C without any problem.

3.2. Microstructure, solvent uptake and conductivity of MCM-41-HPW membranes

Fig. 7 shows the cross-sectional microstructure of mesoporous silica based membranes fabricated by gel-casting technique. As shown in Fig. 7, the density of the membrane increases with the increase in the solid state loading. Besides this, the viscosity of the slurry is found to increase exponentially with the solid state loading [64]. A low viscosity favors the smooth flow of the slurry, suspension homogeneity, degassing, and easy casting, while a high solid state loading is advantageous for obtaining a membrane with lower porosity. The results show that it is possible to obtain HPW/MCM-41 slurry with good flow property and reasonable viscosity by adjusting the solid state loading.

The cross-sectional microstructures of MCM-41-HPW-m membranes fabricated by gel-casting technique are shown in Fig. 8. As shown in Fig. 8(a–f), the membranes do not appear to be dense enough, but is observed to be slightly denser with HPW loading. Fig. 8(g and h) shows the EDS patterns of square regions (area A and area F) of the MCM-41-m and MCM-41-HPW80-m membranes. The Au signal is due to the gold coating applied to the samples prior to the EDS analysis. In the case of MCM-41-m, only Si signal was detected. However, both Si and W signals were detected in the EDS of MCM-41-HPW80-m membrane, indicating that the HPW was supported on meso-porous MCM-41. The comparison of W and Si atomic ratio based on EDS measurement and theoretical calculation of different membranes are summarized in Table 2. The measured W atomic ratios of the membranes are observed to be significantly lower than the theoretical W atomic ratios (Table 2), which imply that there are substantial amount of HPW molecules anchored into the channel of MCM-41 powders. This is consistent with the XRD results.

It is well known that polyacrylic acid has a high affinity for moisture and is hydrophilic. This property is confirmed when the composite membrane is immersed in the distilled water and methanol at 80 °C and a relatively high amount of water and methanol is absorbed. Fig. 9 shows the weight-gain and swelling of pure MCM-41 membrane in pure water and pure methanol as a function of solid state or HPW loading. As shown in Fig. 9a, both water and methanol weight-gain of the membrane decrease with increasing in solid state loading of the formulated slurry, and reach 37% and 27%, respectively (relative to the dry membrane, the same below) when solid state loading was 80 vol.%. The swelling ratios of the membrane also decrease with increasing in the solid state loading, and reaches ~12% both in water and methanol (Fig. 9b), which implies that the membrane will be stable in methanol when used as a fuel. Both water and methanol weight-gain of MCM-41-HPW-m membranes significantly decreases with increasing in

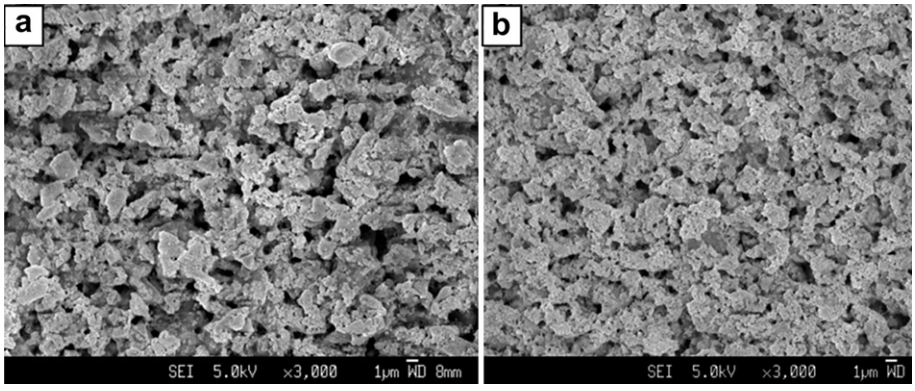

Fig. 7. The cross-sectional microstructure of the pure MCM-41 membranes fabricated by gel-casting as a function of solid state loading (a) 70 vol.%, (b) 80 vol.%.

HPW loading supported on MCM-41 powders (Fig. 9c), which is due to dissolving of HPW initially absorbed on MCM-41 surface.

The proton conductivity measurements of HPW-MCM-41 were characterised by the electrochemical impedance spectroscopy over the frequency range from 1 Hz to 1 MHz between the temperature of 20 and 90 °C under 100% RH. The results were the average of measurements on at least three different samples. The HPW loading in the MCM-41 matrix varied between 0 and 80 wt.%. Fig. 10a shows the proton conductivity of MCM-41-HPW-m membranes as a function of HPW loading measured at different temperatures. In the case of MCM-41-HPW15-m membrane, the conductivity was 2.4×10^{-3} S cm^{-1} and 7.7×10^{-3} S cm^{-1} at 25 °C and 80 °C, respectively. Lu et al. have reported that the proton conductivity of the pristine MCM-41 host is very low, i.e., 5.1×10^{-6} S cm^{-1} [5]. This indicates that the transport of protons through the pure mesoporous silica via surface hydroxyl groups is very difficult. However, the proton conductivity of MCM-41 silica increases significantly with the impregnation and assembly of HPW

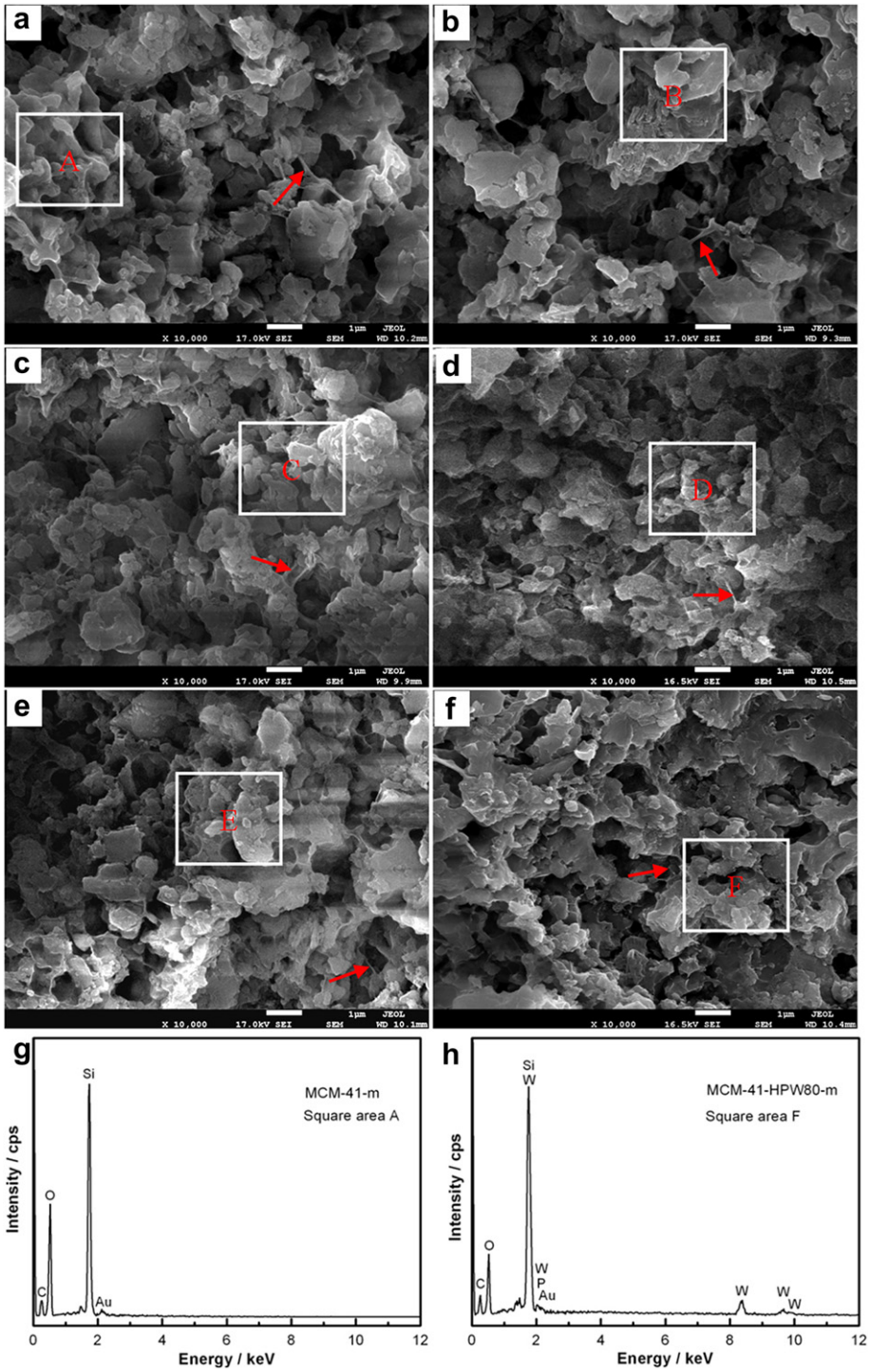

Fig. 8. The cross-sectional microstructure of the MCM-41-HPW-m membranes fabricated by gel-casting with solid state loading 70 vol.% as a function of HPW loading (a) 0 wt.%, (b) 15 wt.%, (c) 30 wt.%, (d) 50 wt.%, (e) 65 wt.%, (f) 80 wt.%, and EDS of (g) area A and (h) area F.

Table 2
Measured and calculated W elements percent of MCM-41-HPW series membranes fabricated by gel-casting technique.

Samples	$(N_w/N_w + N_{Si}) \times 100\%$ Measured results based on EDS test	$(N_w/N_w + N_{Si}) \times 100\%$ Calculated results based on formula
MCM-41-HPW0-m	0 (Square area A Fig. 7a)	0
MCM-41-HPW15-m	0 (Square area B Fig. 7b)	4.21
MCM-41-HPW30-m	1.19 (Square area C Fig. 7c)	6.96
MCM-41-HPW50-m	10.99 (Square area D Fig. 7d)	19.98
MCM-41-HPW65-m	20.15 (Square area E Fig. 7e)	31.72
MCM-41-HPW80-m	29.41 (Square area F Fig. 7f)	50.00

in the MCM-41 structure. For example, the conductivity of MCM-41-HPW80-m membrane was 0.045 S cm^{-1} at 25 °C, which is more than 20 times higher than 2.4×10^{-3} S cm^{-1} measured on MCM-41-HPW15-m membrane. The activation energy of MCM-41-HPW80-m is 11.13 kJ mol^{-1}, which is much smaller than the 18.76 kJ mol^{-1} for MCM-41-HPW15-m. However, the proton conductivity of MCM-41-HPW30-m is 4.4×10^{-3} S cm^{-1} at 25 °C. This value is lower than 0.018 S cm^{-1} as reported by Lu et al. [5], which could be due to the low density of the membrane. Thus, our future work will focus on improving the relative density of the membrane.

Densification and the micro structural optimization of conductive materials are critical in determining the proton or ionic conductivity properties of the electrolyte in fuel cells [46,47]. Fig. 10b shows the proton conductivity of MCM-41-HPW65-m membranes as a function of solid state loading in the slurry for casting membrane. As shown in Fig. 10b, for a fixed HPW loading, the conductivity of membranes increases with increasing in solid state loading, which is directly related to the increase of density of the membrane.

Fig. 10c shows the proton conductivity of MCM-41-HPW65-m membrane fabricated from slurry with solid state loading of 70 vol.% under continuous flow of distilled water on both sides of the membrane at 80 °C. The measured proton conductivity of the membrane is 0.076 S cm^{-1}, which is comparable to the reported results [5,6,12]. The stability of the proton conductivity of PEMs is a very important factor to determine the performance stability of the fuel cells. Fig. 10c shows the conductivity stability of the MCM-41-HPW65-m mesoporous silica composite electrolyte membranes. The conductivity was measured at 80 °C under continuous flow of distilled water on both sides of the electrolyte membranes. The conductivity of the composite membranes decreases rather rapidly initially, but slows down after ~4 h of measurement. The decay in the conductivity is most likely due to the leaching of HPW during the flushing of distilled water. The conductivity stability of MCM-41-HPW65-m composite membrane fabricated by gel-casting technique is also lower than that of HPW/MCM-41 composite membrane fabricated by pressing method reported by Lu et al. [5], which is attributed to the lower density of HPW/MCM-41 (Fig. 8).

To demonstrate the applicability of the HPW/MCM-41 mesoporous silica composites as an inorganic proton-conducting electrolyte in high-temperature PEMs, a single cell was assembled with an MCM-41-HPW65-m membrane of ~0.48 mm in thickness and using PtRu/C catalyst in the anode and Pt/C catalyst in the cathode. The effective area of the cell was 4 cm^2. Fig. 11 shows the cell polarization performance measured at different temperatures in methanol/air without external humidification. The open circuit voltage (OCV) of the cell in methanol/air was ~0.67 V, comparable to 0.68 V reported by Lu et al. [5]. As shown in Fig. 11a, the maximum power output of the cell used MCM-41-HPW30-m membrane is 80 mW cm^{-2} at 150 °C, which is lower than 92 mW cm^{-2} for the cell with VIM-30 wt.% HPW/MCM-41 membrane made by pressing method. In summary, this study indicates that inorganic electrolyte membranes can be fabricated by novel ceramic molding technique and used in the fuel cells, provided that the density of the electrolyte membrane can be enhanced further.

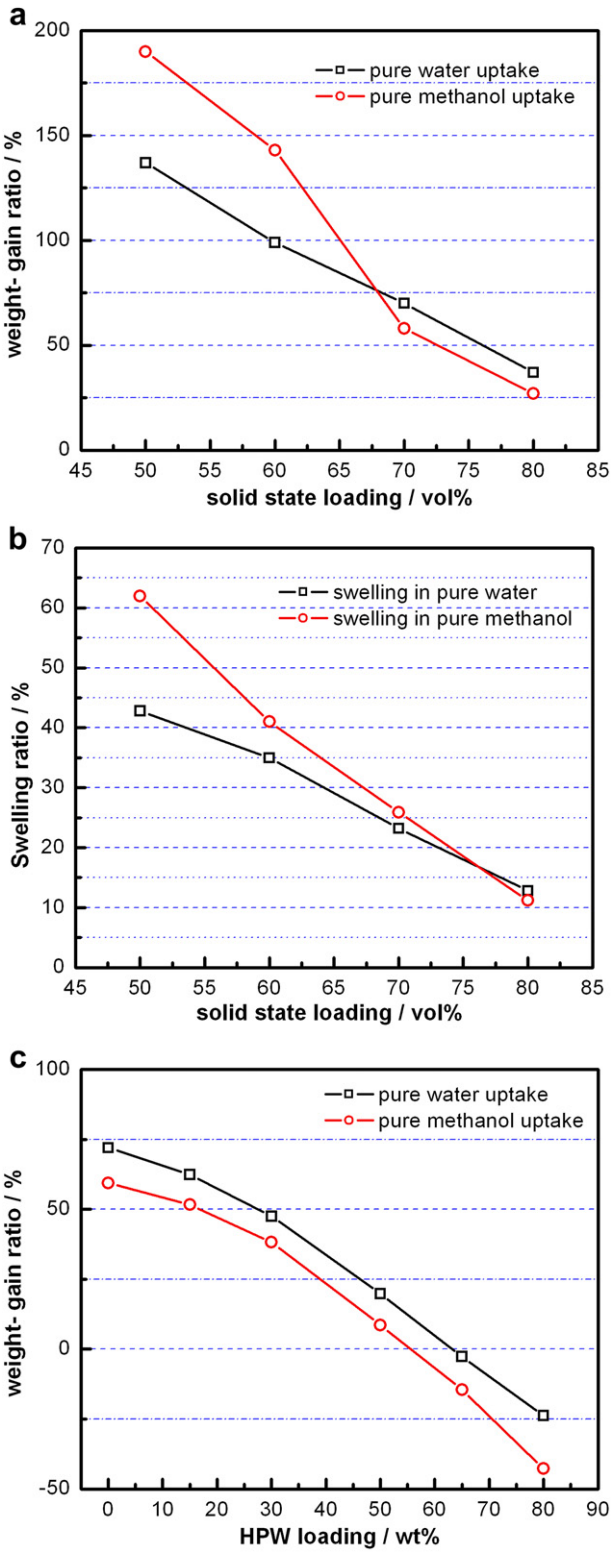

Fig. 9. The (a) weight-gain ratio and (b) swelling ratio of MCM-41 series membranes fabricated by gel casting technique as a function of solid state loading, and (c) weight-gain ratio of MCM-41-HPW-m series membranes as a function of HPW loading in pure water/methanol at 80 °C.

As evidenced in Fig. 11, the maximum power output of cell using MCM-41-HPW65-m electrolyte membrane is 101 mW cm^{-2} at 150 °C (Fig. 11b), which is higher than 80 mW cm^{-2} of cell using MCM-41-HPW30-m electrolyte membrane. This indicates that the cell performance increases with increasing HPW loading in MCM-41 support. The cell performance of MCM-41-HPW65-m electrolyte fabricated by gel-casting technique is slightly lower than

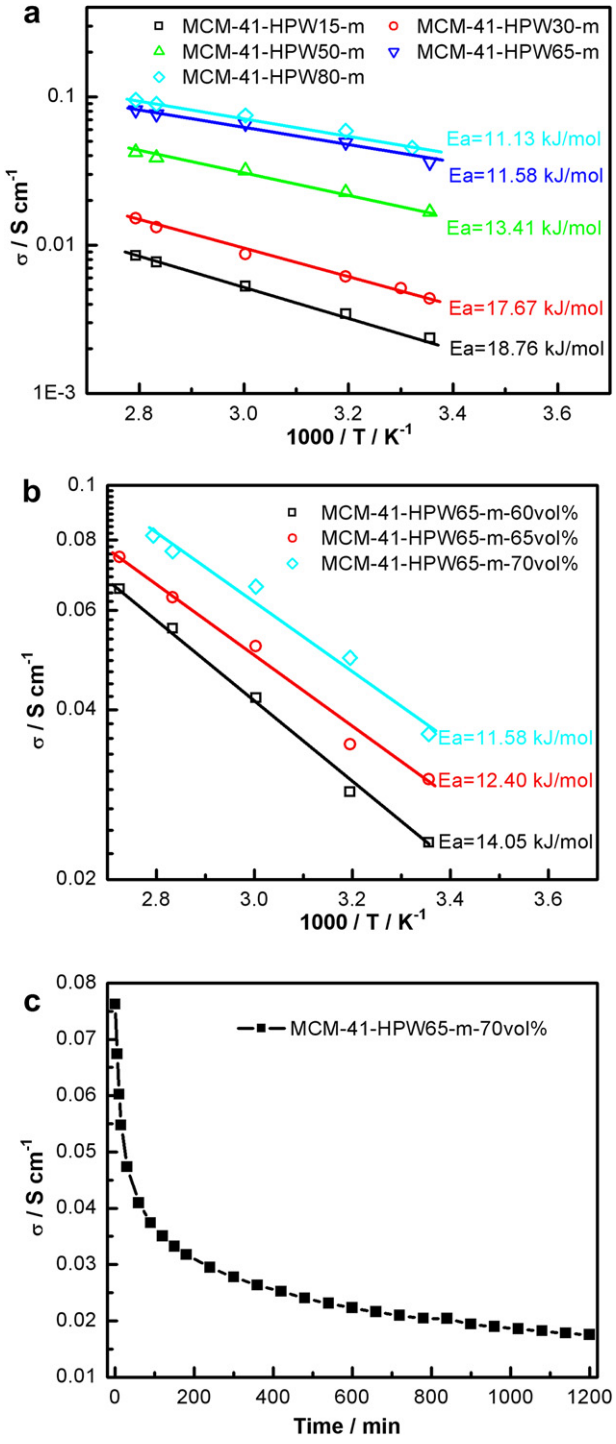

Fig. 10. (a) Conductivity of MCM-41-HPW-m series membrane fabricated by gel-casting technique as a function of HPW loading and a function of test temperature, (b) conductivity of MCM-41-HPW65-m membranes as a function of solid state loading and a function of test temperature, (c) conductivity of MCM-41-HPW65-m membrane as a function of test time under continuous flow of distilled water at both sides of membrane sheet at 80 °C.

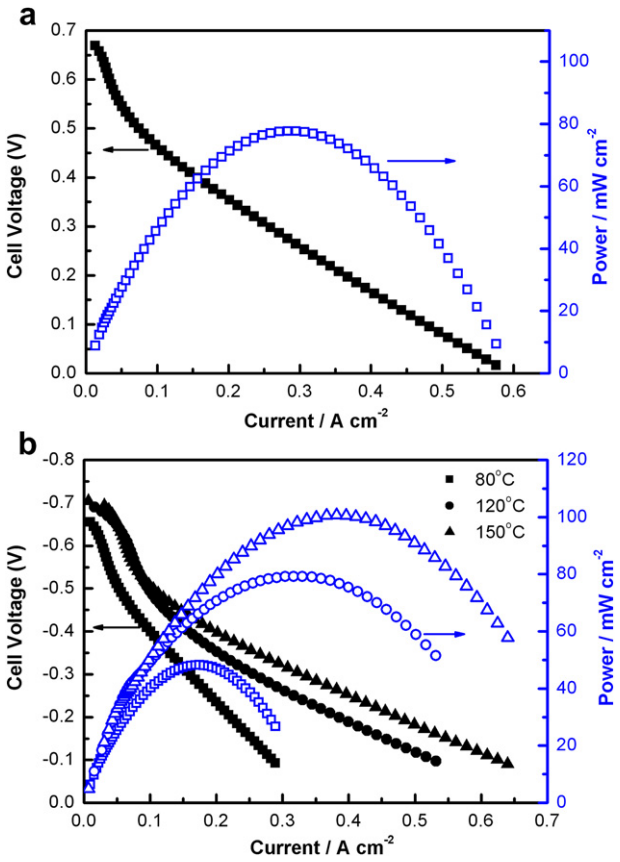

Fig. 11. Polarization curves and power performance of a single cell with (a) MCM-41-HPW30-m electrolyte membrane and (b) MCM-41-HPW65-m electrolyte membrane in methanol/air without external humidification at 150 °C. Air flow rate: 300 mL min^{-1}; methanol solution (2.0 M) flow rate: 1 mL min^{-1}. The membrane thickness was 0.48 mm and made from the slurry with 70 vol.% solid state loading.

115 mW cm^{-2} of that using VIM-67 wt.% HPW/meso-silica electrolyte made by pressing method under the same operating conditions [6]. The difference is attributed to the lower density of the membrane in this case.

4. Conclusion

Gel-casting process has been successfully applied to fabricate HPW/MCM-41 electrolyte membranes. The preliminary results demonstrated that the gel-casting process can be scaled up for the fabrication of thin and large size of HPW/MCM-41 inorganic membrane used in high-temperature PEMFC. The results showed that large amount of loaded HPW is anchored in the mesoporous silica matrix, forming an effective proton conduction pathway. The TGA curve of organic network formed during the gelation stage demonstrated that the composite membrane can operate stably below 200 °C. However, the leaching of HPW during the flushing of the HPW/MCM-41 composite membrane is still an issue. A single cell has been fabricated using the HPW/MCM-41 membrane and produced a maximum power of 101 mW cm^{-2} in methanol/air at 150 °C without humidification. More work will have to be done in future to improve the density of HPW/MCM-41 composite membrane so as to increase the output performance of the fuel cells.

References

[1] C. Yang, S. Srinivasan, A.B. Bocarsly, S. Tulyani, J.B. Benziger, J. Membr. Sci. 237 (2004) 145–161.

[2] Y. Sone, P. Ekdunge, D. Simonsson, J. Electrochem. Soc. 143 (1996) 1254–1259.
[3] A.V. Anantaraman, C.L. Gardner, J. Electroanal. Chem. 414 (1996) 115–120.
[4] T.A. Zawodzinski, T.E. Springer, J. Davey, R. Jestel, C. Lopez, J. Valerio, S. Gottesfeld, J. Electrochem. Soc. 140 (1993) 1981–1985.
[5] S.F. Lu, D.L. Wang, S.P. Jiang, Y. Xiang, J.L. Lu, J. Zeng, Adv. Mater. 22 (2010) 971–976.
[6] J. Zeng, S.P. Jiang, J. Phys. Chem. C 115 (2011) 11854–11863.
[7] A. Sacca, A. Carbone, R. Pedicini, M. Marrony, R. Barrera, M. Elomaa, E. Passalacqua, in: CARISMA Workshop on Ionomer Membranes for Medium and High Temperature Fuel Cells, Stuttgart, Germany, 2008, pp. 225–235.
[8] P. Staiti, M. Minutoli, S. Hocevar, J. Power Sources 90 (2000) 231–235.
[9] X.M. Yan, P. Mei, Y.Z. Mi, L. Gao, S.X. Qin, Electrochem. Commun. 11 (2009) 71–74.
[10] C.C. Chen, H.Y. Tsi, W.C. Tsen, F.S. Chuang, S.C. Jang, Y.C. Shu, S. Wen, C.L. Gong, J. Appl, Polym. Sci. 123 (2012) 1184–1192.
[11] F.J. Shang, L. Li, Y.M. Zhang, H. Li, J. Mater. Sci. 44 (2009) 4383–4388.
[12] H.L. Tang, M. Pan, S.F. Lu, J.L. Lu, S.P. Jiang, Chem. Commun. 46 (2010) 4351–4353.
[13] O. Paschos, J. Kunze, U. Stimming, F. Maglia, J. Phys. Condens. Matter 23 (2011) 1–26.
[14] H.B. Wang, C. Tealdi, U. Stimming, K.L. Huang, L.Q. Chen, Electrochim. Acta 54 (2009) 5257–5261.
[15] H.B. Wang, C. Tealdi, K.L. Huang, U. Stimming, L.Q. Chen, J. Alloys Compd. 485 (2009) L28–L30.
[16] X.L. Chen, C.R. Xia, U. Stimming, Electrochim. Acta 52 (2007) 7835–7840.
[17] X.L. Chen, X. Li, S.A. Jiang, C.R. Xia, U. Stimming, Electrochim. Acta 51 (2006) 6542–6547.
[18] L.J. Liu, H.Y. Tu, C. Cremers, U. Stimming, Solid State Ionics 177 (2006) 2417–2419.
[19] T. Uma, H.Y. Tu, S. Warth, D. Schneider, D. Freude, U. Stimming, J. Mater. Sci. 40 (2005) 2059–2063.
[20] T. Uma, H.Y. Tu, D. Freude, D. Schneider, U. Stimming, J. Mater. Sci. 40 (2005) 227–230.
[21] T. Kenjo, Y. Ogawa, Solid State Ionics 76 (1995) 29–34.
[22] Y.Z. Jiang, X.X. Xu, R. Lan, L. Zhang, S.W. Tao, J. Alloys Compd. 480 (2009) 874–877.
[23] Y.Z. Jiang, T. Matthieu, R. Lan, X.X. Xu, P.I. Cowin, S.W. Tao, Solid State Ionics 192 (2011) 108–112.
[24] T. Matsui, S. Takeshita, Y. Iriyama, T. Abe, M. Inaba, Z. Ogumi, Electrochem. Commun. 6 (2004) 180–182.
[25] X.L. Chen, C.S. Wang, E.A. Payzant, C.R. Xia, D. Chu, J. Electrochem. Soc. 155 (2008) B1264–B1269.
[26] P. Heo, M. Nagao, T. Kamiya, M. Sano, A. Tomita, T. Hibino, J. Electrochem. Soc. 154 (2007) B63–B67.
[27] P. Heo, N. Kajiyama, K. Kobayashi, M. Nagao, M. Sano, T. Hibino, Electrochem. Solid-State Lett. 11 (2008) B91–B95.
[28] M. Nagao, T. Kamiya, P. Heo, A. Tomita, T. Hibino, M. Sano, J. Electrochem. Soc. 153 (2006) A1604–A1609.
[29] P. Heo, H. Shibata, M. Nagao, T. Hibino, M. Sano, J. Electrochem. Soc. 153 (2006) A897–A901.
[30] M. Nagao, A. Takeuchi, P. Heo, T. Hibino, M. Sano, A. Tomitab, Electrochem. Solid-State Lett. 9 (2006) A105–A109.
[31] M. Misono, Mater. Chem. Phys. 17 (1987) 103–120.
[32] M. Misono, Cat. Rev. Sci. Eng. 29 (1987) 269–321.
[33] N. Mizuno, M. Misono, Chem. Rev. 98 (1998) 199–217.
[34] S. Soled, S. Miseo, G. McVicker, W.E. Gates, A. Gutierrez, J. Paes, Catal. Today 36 (1997) 441–450.
[35] K.D. Kreuer, Chem. Mater. 8 (1996) 610–641.
[36] Y.S. Kim, F. Wang, M. Hickner, T.A. Zawodzinski, J.E. McGrath, J. Membr. Sci. 212 (2003) 263–282.
[37] D.E. Katsoulis, Chem. Rev. 98 (1998) 359–387.
[38] O.O. Omatete, M.A. Janney, R.A. Strehlow, Am. Ceram. Soc. Bull. 70 (1991) 1641–1649.
[39] M.A. Janney, O.O. Omatete, C.A. Walls, S.D. Nunn, R.J. Ogle, G. Westmoreland, J. Am. Ceram. Soc. 81 (1998) 581–591.
[40] A.C. Young, O.O. Omatete, M.A. Janney, P.A. Menchhofer, J. Am. Ceram. Soc. 74 (1991) 612–618.
[41] L. Zhang, S.P. Jiang, W. Wang, Y.J. Zhang, J. Power Sources 170 (2007) 55–60.
[42] L. Zhang, Y.J. Zhang, Y.D. Zhen, S.P. Jiang, J. Am. Ceram. Soc. 90 (2007) 1406–1411.
[43] L. Zhang, S.P. Jiang, C.S. Cheng, Y.J. Zhang, J. Electrochem. Soc. 154 (2007) B577–B582.
[44] S.P. Jiang, L. Zhang, Y.J. Zhang, J. Mater. Chem. 17 (2007) 2627–2635.
[45] C.S. Cheng, L. Zhang, Y.J. Zhang, S.P. Jiang, Solid State Ionics 179 (2008) 282–289.
[46] S.P. Jiang, L. Zhang, H.Q. He, R.K. Yap, Y. Xiang, J. Power Sources 189 (2009) 972–981.
[47] L. Zhang, H.Q. He, H.W. Wu, C.Z. Li, S.P. Jiang, Int. J. Hydrogen Energy 36 (2011) 6862–6874.
[48] C.T. Kresge, M.E. Leonowicz, W.J. Roth, J.C. Vartuli, J.S. Beck, Nature 359 (1992) 710–712.
[49] A. Corma, A. Martinez, V. Martinez-Soria, J. Catal. 169 (1997) 480–489.
[50] J.S. Beck, J.C. Vartuli, W.J. Roth, M.E. Leonowicz, C.T. Kresge, K.D. Schmitt, C.T.W. Chu, D.H. Olson, E.W. Sheppard, S.B. McCullen, J.B. Higgins, J.L. Schlenker, J. Am. Ceram. Soc. 114 (1992) 10834–10843.
[51] S.M. Jin, G.Z. Qiu, F. Xiao, Y. Chang, C.F. Wan, M. Yang, J. Am. Ceram. Soc. 90 (2007) 957–961.
[52] J. Yang, M.J. Janik, D. Ma, A.M. Zheng, M.J. Zhang, M. Neurock, R.J. Davis, C.H. Ye, F. Deng, J. Amer. Chem. Soc. 127 (2005) 18274–18280.
[53] A.S. Khder, H.M.A. Hassan, M.S. El-Shall, Appl. Catal. A: Gen. 411 (2012) 77–86.
[54] Y. Zheng, Z.H. Li, X. Shen, L.X. Lin, Mater. Lett. 60 (2006) 3221–3223.
[55] A.S. Dias, M. Pillinger, A.A. Valente, Micropor. Mesopor. Mater. 94 (2006) 214–225.
[56] F. Lefebvre, J. Chem. Soc. Chem. Commun. (1992) 756–757.
[57] Y. Liu, L. Xu, B.B. Xu, Z.K. Li, L.P. Jia, W.H. Guo, J. Mol, Catal. A Chem. 297 (2009) 86–92.
[58] G. Kamalakar, K. Komura, Y. Sugi, Appl. Catal. A Gen. 310 (2006) 155–163.
[59] G. Kamalakar, K. Komura, Y. Kubota, Y. Sugi, J. Chem. Technol. Biotechnol. 81 (2006) 981–988.
[60] J. Kaur, K. Griffin, B. Harrison, I.V. Kozhevnikov, J. Catal. 208 (2002) 448–455.
[61] I.V. Kozhevnikov, Chem. Rev. 98 (1998) 171–198.
[62] G.S. El-Bahy, E.M. Abdelrazek, M.A. Allam, A.M. Hezma, J. Appl. Polym. Sci. 122 (2011) 3270–3276.
[63] M.A. Moharram, M.A. Allam, J. Appl. Polym. Sci. 105 (2007) 3220–3227.
[64] L. Zhang, H.Q. He, W.R. Kwek, J. Ma, E.H. Tang, S.P. Jiang, J. Am. Ceram. Soc. 92 (2009) 302–310.